Marine Structures 103 (2025) 103832

Contents lists available at ScienceDirect

Marine Structures

journal homepage: www.elsevier.com/locate/marstruc

Implementation of seismic soil-structure interaction in OpenFAST and application to an offshore wind turbine on jacket structure

Amir M. Kaynia [a,b,*], Daniel Martens Pedersen [b], Henrik Askheim [c], Carlos Romero-Sánchez [d]

[a] Norconsult AS, Sandvika, Norway
[b] Norwegian Geotechnical Institute (NGI), Oslo, Norway
[c] Aas-Jakobsen AS, Oslo, Norway
[d] SIANI, University of Las Palmas de Gran Canaria (ULPGC), Las Palmas de Gran Canaria, Spain

ARTICLE INFO

Keywords:
Offshore wind turbine
OpenFAST
Soil-structure interaction
Earthquake response
Jacket structure

ABSTRACT

One of the challenges in design of offshore wind turbines (OWTs) is that the analyses are performed using specialized software dedicated to hydro-aero-servo-elasto-dynamic analyses which often cannot rigorously perform seismic soil-structure interaction (SSI) analyses. This work presents a methodology to extend these tools to include seismic SSI analyses in these tools with a specific application in the open source OWT analysis tool OpenFAST. The developed method is applied to 10 MW offshore wind turbine on a jacket structure founded on piles. The SSI is implemented using a multi-step sub-structuring method. The method is based on the SSI stiffness and kinematic interaction. The jacket base is attached to pile foundation springs, and excited by forces calculated from the pile-head motions during the earthquake. The spring stiffness and pile-head motions can be determined using well-established methods. In this, they are obtained using the finite element program Abaqus. A complementary integrated Abaqus model of the jacket and tower is then used to verify the implementation of the multi-step method in OpenFAST. The IEA 10 MW reference OWT established in the European research project INNWIND is used in the verification. Using the developed model, the study then attempts to investigate some of the characteristic earthquake responses of the OWT structure. Simulations show how the top of tower displacements are dominated by the wind-induced forces during production form the rotor-nacelle-assembly, while the tower top accelerations and base overturning moments are dominated by the earthquake-induced loads.

1. Introduction

The offshore wind farm developments in areas prone to seismic action, such as Taiwan, China, Japan and North America, has made the industry question the performance of offshore wind turbine (OWT) foundations due to earthquake loading. The most common and cost-effective foundation solution is the monopile foundation, which has been developed and well tested over the last three decades in the less seismic active areas of Northern Europe. A piled jacket structure has been proposed as an alternative solution, which has been shown to perform well in terms of handling the overturning moments at the structure base.

* Corresponding author.
E-mail address: amir.m.kaynia@ngi.no (A.M. Kaynia).

https://doi.org/10.1016/j.marstruc.2025.103832
Received 27 June 2024; Received in revised form 12 March 2025; Accepted 10 April 2025
Available online 18 April 2025
0951-8339/

The influence of SSI plays a fundamental role in the dynamics and the seismic response of the support structures. The soil-foundation flexibility can affect the natural frequency and damping of the system and reducing the impact of the earthquake loading. Numerous studies have shown the importance of SSI on the seismic response of wind turbines [1–3], and the relevance of kinematic interaction in the seismic analysis of OWTs [4,5].

The seismic analysis of OWTs can be carried out using linear or nonlinear solutions. For linear (or slightly nonlinear) soil response, traditionally the impedances functions (often known as dynamic stiffnesses in the SSI community) are utilized at the interface between the structure and foundation. Some of the existing solutions are based on frequency domain dynamic analysis of piles embedded in a homogeneous or layered half-space using simplified or advanced boundary integral formulations for the soil together with the finite element method for the piles [6–8,3]. Furthermore, an effective approach is the lumped parameter model [9–11]. This method allows in addition use of SSI impedance in time domain simulations. Daamgaard et al. [9] used semi-analytic frequency-domain solutions to evaluate the dynamic impedance functions of the pile-soil system to calibrate a lumped parameter model for integration into an aeroelastic code. Andersen [11] developed a frequency-independent consistent lumped parameter models for structures with two or more foundations. Other researchers have employed simplified models for piles, represented by a matrix of constant springs [12–14].

On the other hand, nonlinear SSI models are commonly used in dynamic and seismic analyses of OWTs [1,2,15,16], where more often Winkler models are used which characterize the soil by uncoupled nonlinear springs, commonly known as *p-y* curves, originally developed for piles in the oil and gas industry [17]. Yang et al. [1] investigated the effect of nonlinear soil behaviour on the structural response of offshore wind turbines subjected to wind, waves and earthquake loads. They also studied the impact of the misalignment between the direction of the ground motion and that of the wind load. Shi et al. [2] showed that the nonlinear pile-soil interaction has a remarkable impact on the dynamic and seismic response of offshore wind turbines. Other researchers have used macro-element models which in simplest form condense the response of the foundation and the soil to a nonlinear force-displacement relation at the interface between the foundation and the superstructure. Krathe and Kaynia [18] implemented a nonlinear macro-element foundation model in FAST [19]. The nonlinear response was captured using a multi-surface kinematic hardening model, by the combination of parallel elasto-plastic springs originally proposed by Iwan [20]. Bergua et al. [21] implemented in OpenFAST [22] an elastoplastic, macro-element model [23] with kinematic hardening, which captures the stiffness and damping characteristics of the foundations more accurately than the more traditional and simplified SSI modelling approaches.

See Kaynia [24] for a review of the various linear and nonlinear spring methods along with other design issues with special significance to OWTs such as the effect of vertical earthquake shaking.

A considerable number of studies have been conducted on OWTs founded on monopile substructure [25–28], however, there are only a few studies that have addressed the earthquake effect on OWTs on jacket substructures. Gelagoti et al. [29] have studied nonlinear soil effects of a 10 MW OWT founded on both a monopile and a jacket substructure. Both models were excited by different earthquake acceleration time series. The results show that the accumulated foundation rotation is larger for the monopile than for the jacket. Ngo and Kim [30] compared the seismic performance of different types of offshore foundations. Fragility analysis confirmed that the seismic intensity influences the vulnerability of OWT systems. The jacket exhibited lower horizontal displacements at the mudline than the monopile substructure, although the jacket was the most sensitive in terms of tower-base moment, as serious stresses may occur at the base of the tower, that is, near the transition piece (TP).

Alati et al. [31] analysed the seismic response of a jacket-supported OWT considering different load cases using the aero-elasto-dynamic code BLADED [32]. The study showed that seismic loading may cause a significant increase of stresses, demonstrating the need for a seismic assessment in sites prone to earthquakes. Abhinav and Saha [33] studied the nonlinear dynamic behaviour of jacket-supported OWTs, highlighting that ignoring SSI effects can lead to an overestimation of the structural loads. Ku and Chien [34] presented a study of load bearing characteristics of a jacket foundation pile for an OWT offshore Taiwan. They noted that the foundation deformation computed from the ultimate loads of a 475-year return period event may exceed the allowable foundation deformation, which indicates that the jacket foundation may fail in this specific case. Later, Ju and Huang [35] proposed an analysis framework for jacket-supported offshore wind turbines. The results showed that the design of the jacket members is controlled by the combination of the environmental and seismic loads during power production. James and Haldar [36] analysed the seismic vulnerability of a jacket supported large OWT using Abaqus [37]. They highlighted the relevance of considering higher modes and multi-directional ground shaking on the dynamic response of OWTs. Romero-Sanchez and Padrón [38] studied the influence of the direction of the wind and seismic loads on the structural response of a four-legged jacket- supported OWT. They concluded that load combinations with aligned wind and ground motion directions are often not the worst-case scenario.

Some of the studies mentioned above were based on nonlinear aero-hydro-servo-elastic simulations. In this field, one of the most popular codes is OpenFAST [22] which is an open-source tool for simulating the coupled dynamic response of wind turbines in time domain. Currently, the code does not provide the possibility to include SSI for earthquake loads. There is the possibility to consider SSI and seismic loads through coupling with other software [39–41]. Plopradit et al. [39] studied the dynamic behaviour in operating conditions of a jacket substructure including SSI by replacing the sub-structural module in FAST with the component of offshore substructure in X-SEA. Yan et al. [40] used FAST to analyse wind and wave loads, which were fed into the finite element software ANSYS. The finite element model made it possible to consider the nonlinear SSI effects and earthquake loading in the jacket substructure. Another option is to modify the OpenFAST modules. Romero-Sanchez and Padrón [42] modified SubDyn [43] module to implement multi-support ground input motion and dynamic SSI through a lumped parameter model. Wang and Ishihara [44] developed a new FounDyn module in OpenFAST to consider the foundation dynamics. This module is currently not available in OpenFAST.

The main objective of this paper is to propose and verify a new methodology for including the seismic SSI effects in a rigorous manner in OpenFAST which would allow simultaneous consideration of environmental and earthquake loading. An apparently similar approach was applied in [42] in which the conventional three-step method based on the kinematic and inertial interactions was used. This approach, however, requires modification of the source code of the SubDyn module and changing the input files in OpenFAST to allow for imposing the ground accelerations at the base of the superstructure. Moreover, it requires addition of Lumped Parameter Models to account for SSI which demands a major implementation effort. In the present formulation, the kinematic interaction motions are converted to equivalent forces that can directly be applied to the base of the superstructure with no need for additional coding in OpenFAST. This approach can be readily extended to multi-directional shaking and for inclusion of radiation damping in the foundation as described in the next section. Using the developed formulation and implementation, the study then attempts to investigate some of the characteristic earthquake responses of OWTs on jacket structures.

It should be noted that the proposed method applies strictly speaking to linear soil response or moderately nonlinear response which can be approximated through the equivalent linear concept. The interaction between the soil/foundation and the structure is incorporated though SSI springs and kinematic interaction forces. Because the soil medium is not explicitly included in the computational model, extreme nonlinear soil behavior cannot be considered. Such behaviors are present only in certain soils under strong shaking (such as liquefaction in loose sandy soils and stiffness/strength degradation in soft clays). For these conditions, nonlinear finite element (FE) tools should be used; for example, Abaqus which is used in this study to highlight the role of soil nonlinearity under strong shaking. Except for limited wind park locations with such extreme conditions, OWTs are installed in areas with relatively good soil conditions for which use of equivalent linear soil models provides a reliable picture of the seismic response. More discussion on this subject, especially the impact of strong soil nonlinearity is included in Section 6.

1.1. Modelling approach

Incorporation of the complex geometry and loading of an OWT makes the aero-hydro-servo-elastic computational software OpenFAST [22] highly relevant for this research. OpenFAST is custom made for simulating the environmental loads and dynamics of wind turbines, including waves, current and submerged effects for an offshore structure. However, OpenFAST lacks the possibility of connecting a soil domain to the OWT structure. This leads to the choice of two complementary models; (1) an OpenFAST model attached to springs representing the pile and soil foundation, and (2) a fully integrated finite element model including both structure and soil. The latter is made in the finite element analysis tool Abaqus [37], in which the geometry of the RNA is included only as added mass and mass moment of inertia.

The Abaqus model is used in this study for two purposes: a) to provide the soil-foundation springs and kinematic interaction input to the structure modelled in OpenFAST, and b) to verify the results of the implemented solution in OpenFAST against those of fully integrated soil-structure system modelled in Abaqus.

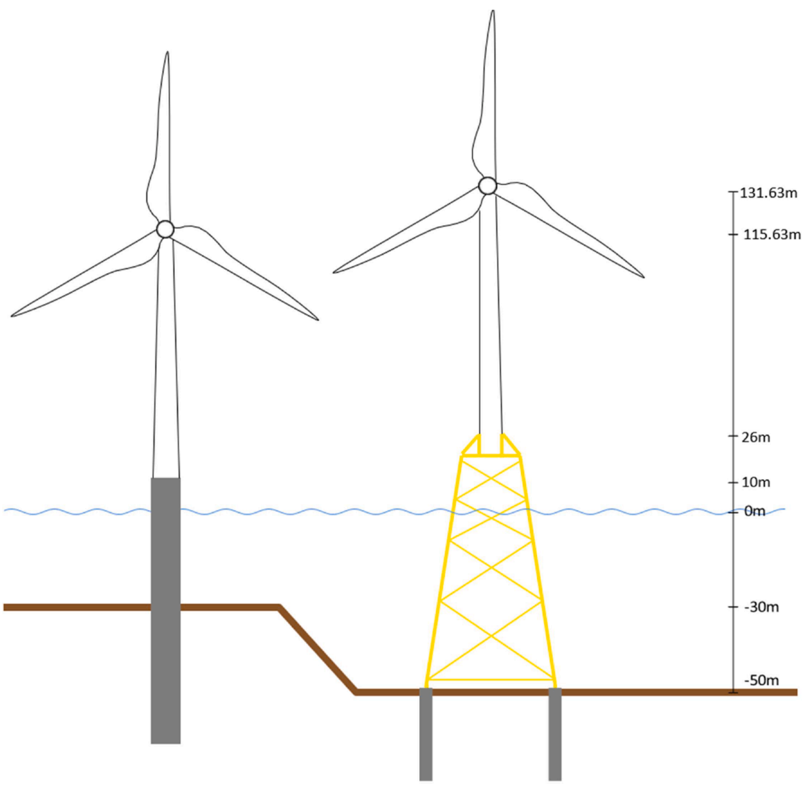

Fig. 1. Illustration of IEA OWT placed on reference jacket.

2. Problem definition

2.1. The reference offshore wind turbine

The structure analysed in this study is an OWT on a four-legged steel jacket support structure. The OWT design used is based on the International Energy Agency's (IEA) 10 MW OWT [45], which is a further development of the 10 MW reference wind turbine (RWT) [46] referred to as the DTU 10 MW RWT, developed by the Danish Technical University. The jacket design is based on Rambøll's reference jacket design from the European research project INNWIND [47]. The jacket is mounted on friction piles; however, no pile design is presented other than a design in a preliminary report in the INNWIND project presented by Rambøll [48]. This pile design is therefore used along with the reference jacket in this study. Different types of TP could be used for such constructions; the project has presented a generic strutted steel beam TP along with the reference jacket, which suit its purpose in the present study.

For the present research an adaptation has been made to the design. The reference jacket is made for the DTU 10 MW RWT rather than the further developed IEA 10 MW OWT. The latter OWT design is based on a monopile foundation with a different foundation/tower intersection level than for the jacket and with a larger RNA, but with the same hub height. Indeed, the IEA tower and RNA structure have about double the mass compared to the structure designed by Rambøll for the reference jacket. However, as the focus of the present study is on the seismic analysis methodology rather than optimization of the structure, the chosen design is considered suitable for the purpose. Fig. 1 shows an illustration of the IEA OWT placed on the reference jacket and Table 1 summarizes the key dimensions of the structure.

The four piles penetrate 42 m below the mudline. The outer diameter is the same for the whole pile, however, different sections have different wall-thickness [49]. The steel material properties used for piles and jacket are Young's modulus = 210 GPa, Poisson's ratio = 0.3 and mass density = 7850 kg/m^3. Details of the soil profile employed in this study is presented in Table 2.

2.2. Earthquake shaking

For the seismic analyses, the acceleration time history of the Loma Prieta earthquake recorded at the Menhaden Court, Foster City, on 18th of October 1989, from the PEER Strong Motion Database [50] was used. Fig. 2 shows the horizontal acceleration of the north-south (N-S) and the east-west (E-W) components together with their acceleration response spectra. The peak ground accelerations (PGA) are about 0.11 g in both directions.

2.3. Environmental loads

The aerodynamic loads on the blades and the tower were calculated by AeroDyn [51]. The full field wind data was made with the use of turbulence spectral models; the model used in the present study was the Kaimal spectral model. Because the rated wind speed for the turbine [46] was 11 m/s, the wind field made by TurbSim [52] was set to have a mean wind speed of 11 m/s at the reference height. The reference height was set at the hub at 131.6 m above mean sea level. The wind direction was set to be along the x-axis such that the motion is mainly in the N-S direction of the earthquake.

The wave loads in OpenFAST are given through the module HydroDyn [53] where the wave kinematics model is chosen and defined. For the irregular waves, the JONSWAP spectrum was used since the sea state is considered developing when there are high wind speeds blowing on the wind turbine. The significant wave height H_S and spectral wave period T_P were set to 8 m and 12 s, respectively.

3. Methodology for soil-structure interaction

As stated earlier, OpenFAST does not include a soil foundation system. The soil-structure interaction in OpenFAST is therefore implemented in the presented study by a sub-structuring approach. The SSI through the foundation (that is, pile and soil) is then

Table 1
Key dimensions of the modelled structure.

Rating [MW]	10
Hub height [m]	131.6
Tower length [m]	105.6
Tower top diameter, wall thickness [m]	5.50, 0.03
Tower base diameter, wall thickness [m]	8.30, 0.07
Jacket length (not including TP) [m]	66.5
Jacket top width [m]	14
Jacket base width [m]	34
Transition piece length [m]	8
Pile outer diameter [m]	2.438
Pile length [m]	43.5
Pile soil penetration [m]	42

Table 2
Properties of soil profile [49].

Layer	Thickness [m]	Mass density [kg/m2]	Young's modulus [MPa]	Poisson's ratio [-]	Shear strength [kPa]
1	2	1936	34.4	0.3	1.8
2	3.5	1936	66.6	0.3	6.8
3	3.5	1936	92.6	0.3	13.1
4	1	1936	106	0.3	17.1
5	5	1936	122	0.3	22.5
6	5	2038	192	0.3	32.0
7	2.5	2089	241	0.3	39.6
8	6.5	2140	300	0.3	49.4
9	5	2140	336	0.3	62.1
10	4	2140	362	0.3	72.0
11	2	2140	378	0.3	78.6
12	10	2140	409	0.3	91.8
13	10	2140	455	0.3	113.8
14	10	2140	497	0.3	135.8
15	10	2140	536	0.3	157.8
16	10	2140	572	0.3	179.8

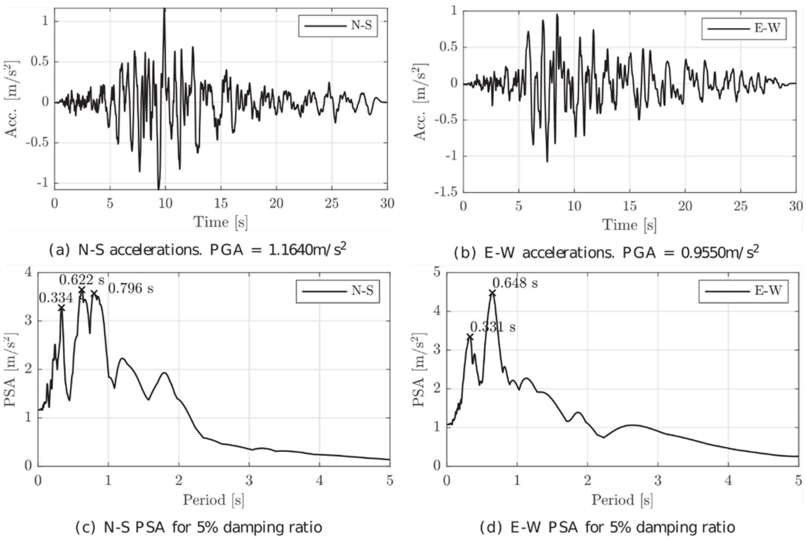

Fig. 2. Loma Prieta earthquake recorded at Menhaden Court, Foster City, 18th of October 1989. (a) and (b) acceleration time series, (c) and (d) acceleration response spectra.

represented by linear springs attached to the bottom of the jacket legs. The effects of radiation damping and added mass from the foundation will then not be included in the dynamics. Both these effects are negligibly small for the typical SSI frequencies involved [6]. However, if it is of special interest, for example evaluation of higher modes on the turbine response or assessment of fatigue in diagonal elements of the jacket, then it is straightforward to use the complex impedance matrices and compute an added soil mass and a radiation damper constant. Computation and implementation of these parameters has been illustrated by Kjørlaug and Kaynia [25]. To apply earthquake load in OpenFAST, the best approach is to apply seismic load as a time series of forces. The forces are obtained using the foundation springs and the time series of pile top displacements and rotations due to the kinematic interaction.

The equation of motion describing the dynamic response of the substructure in the SubDyn module can be written as:

$$[M]\{\ddot{u}(t)\} + [C]\{\dot{u}(t)\} + [K]\{u(t)\} = \{F(t)\} \tag{1}$$

where $[M]$, $[C]$ and $[K]$ are the global mass, damping and stiffness matrices, respectively, and $\{u\}$, $\{\dot{u}\}$ and $\{\ddot{u}\}$ are column vectors holding the displacement degrees of freedom (DOF) and their time derivatives. In this case, the matrix $[K]$ contains the contribution of the specified $[K_{SSI}]$ whose matrix entries are directly added to the proper DOFs of the stiffness matrix. $\{F\}$ are the external forces at all DOFs of the assembled system.

The motion vector can be written to separate the response quantities from the seismic input [54]:

$$u(t) = u^t(t) - u_g(t) \tag{2}$$

where u^t represents total displacements and u_g contains the components of the ground displacements. The forces are composed of loads that are accounted for by SubDyn, such as the gravity, and external loads acting on the substructure from additional modules, including hydrodynamic loads, forces from the tower and seismic forces (F_{SSI}). The latter can be determined from the following expression and transferred to the right-hand side of the equation of motion, that is.

$$F_{SSI}(t) = [K_{SSI}]\{u_g(t)\} \tag{3}$$

$$[M]\{\ddot{u}(t)\} + [C]\{\dot{u}(t)\} + [K]\{u(t)\} = \{F(t)\} + \{F_{SSI}(t)\} \tag{4}$$

To be strictly rigorous, one should also include the corresponding load vector from damping matrix, that is, $[C_{SSI}]\{\dot{u}_g(t)\}$ in Eq. (3). However, earlier studies (For example, [4]) have shown that the contribution by damping from piles for the typical SSI frequencies involved are practically negligible. If considered useful, for example in the evaluation of the fatigue in diagonal ties characterized by higher frequencies, the damping force vector can easily be included by using the damping matrix, which can be computed by a variety of simple and of elasto-dynamic tools (for example, [6]), and the pile response velocity vector. While the methodology and its application is presented for horizontal earthquake shaking, the approach can be readily extended to vertical shaking by considering the vertical SSI springs and the kinematic pile response.

The substructure is modelled as a linear frame finite-element model with Timoshenko beams. In a finite- element analysis of a typical multi member structure the number of degrees of freedom could seriously slow down the computations. Therefore, the Craig-Bampton [55] (C-B) systems reduction is used which divides the equations of motion into interior and boundary (subscript B) DOFs. The C-B method reduces the number of the internal generalized degrees of freedom of the substructure (subscript m):

$$\begin{bmatrix} \widetilde{M}_{BB} & \widetilde{M}_{Bm} \\ \widetilde{M}_{mB} & I \end{bmatrix} \begin{Bmatrix} \ddot{u}_{TP}(t) \\ \ddot{q}_m(t) \end{Bmatrix} + \begin{bmatrix} \widetilde{C}_{BB} & \widetilde{C}_{Bm} \\ \widetilde{C}_{mB} & \widetilde{C}_{mm} \end{bmatrix} \begin{Bmatrix} \dot{u}_{TP}(t) \\ \dot{q}_m(t) \end{Bmatrix} + \begin{bmatrix} \widetilde{K}_{BB} & 0 \\ 0 & K_{mm} \end{bmatrix} \begin{Bmatrix} u_{TP}(t) \\ q_m(t) \end{Bmatrix} = \begin{Bmatrix} \widetilde{F}_{TP}(t) \\ F_m(t) \end{Bmatrix} + [K_{SSI}]\{u_g(t)\} \tag{5}$$

where the overhead bar denotes matrices and vectors considering the fixed-bottom boundary conditions and subscript TP represents

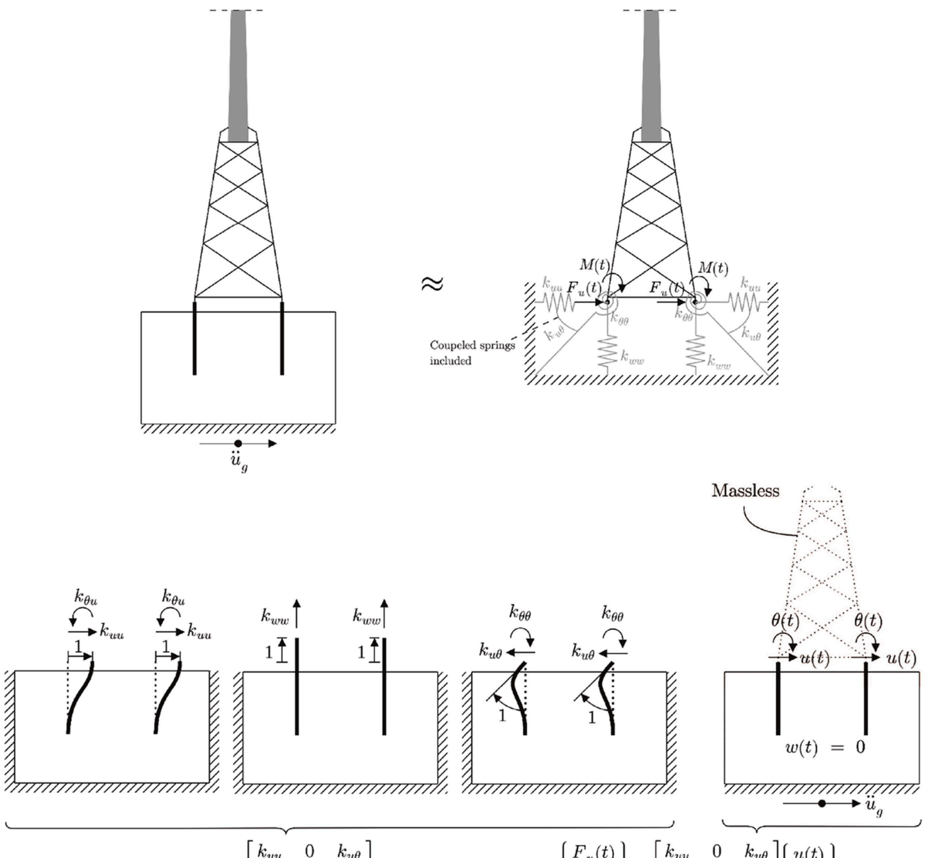

$$[\mathrm{K}] = \begin{bmatrix} k_{uu} & 0 & k_{u\theta} \\ 0 & k_{ww} & 0 \\ k_{\theta u} & 0 & k_{\theta\theta} \end{bmatrix} \qquad \{\mathrm{F}\} = \begin{Bmatrix} F_u(t) \\ F_w(t) \\ M(t) \end{Bmatrix} = \begin{bmatrix} k_{uu} & 0 & k_{u\theta} \\ 0 & k_{ww} & 0 \\ k_{\theta u} & 0 & k_{\theta\theta} \end{bmatrix} \begin{Bmatrix} u(t) \\ w(t) \\ \theta(t) \end{Bmatrix} = [\mathrm{K}]\{\mathrm{u}\}$$

Fig. 3. Schematics of implemented sub-structuring method demonstrated for simplicity for a 2D case.

forces and displacements at the transition piece.

Combining the steps of sub-structuring method to represent the SSI effects relies upon the principle of superposition, which would not strictly apply if non-linear soil effects were included. Thus, even though OpenFAST has the capacity of utilizing a non-linear solver, soil non-linearities cannot be rigorously included by this method (a practical approach to extend the method to compute approximate nonlinear earthquake response is discussed in Section 6).

The above sub-structuring procedure is schematically illustrated in Fig. 3 and described in the list below, where the Abaqus model is utilized for the first two steps (NB: other simpler methods could be used for these steps; however for a consistent verification of the implemented procedure the required data are derived with the same computational tool):

1) Extract the pile top (foundation) stiffness matrix: Apply unit displacement/rotation at one degree of freedom (DOF), restraining motion at the other DOFs. The computed reaction forces at these DOFs constitute the foundation stiffness matrix. The boundaries of the soil profile are fixed for this step which is illustrated for a 2D system on the bottom left side in Fig. 3.
2) To obtain the kinematic interaction motions at the top of the piles, the horizontal earthquake shaking is applied to the base of the soil model with the tied boundary conditions on the lateral sides of the model, and including a massless jacket to capture the correct behaviour of the foundation while excited by an earthquake. The earthquake forces at the pile tops are then obtained by multiplying the time series with the stiffness matrix computed in step 1. This step is illustrated on the bottom right side in Fig. 3. Each jacket leg is attached to the ground through the obtained foundation springs, and the earthquake load is applied by the force time series at the bottom of each jacket leg. This step is illustrated for a 2D in the top right in Fig. 3.
3) Apply the earthquake load to the structure: the ServoDyn [56] input file in OpenFAST is modified to allow for the structural control to apply a time series of loads and moments. The switch for number of substructure structural control is set to four since there are four reaction nodes in the model.

Fig. 3 shows for simplicity of illustration the procedure for a 2D system. As the real model is 3D, with 6 DOFs at each node, the stiffness matrix attached to each jacket leg will have the size 6 × 6 including the DOFs for the axial and torsional motions. The computed stiffness matrix of the soil-structure interaction described in Section 2, [K_{SSI}] is:

$$[K_{SSI}] = \begin{bmatrix} 4.69 & 0.0 & 0.0 & 0.0 & -19.35 & 0.0 \\ 0.0 & 4.69 & 0.0 & 19.35 & 0.0 & 0.0 \\ 0.0 & 0.0 & 24.45 & 0.0 & 0.0 & 0.0 \\ 0.0 & 19.35 & 0.0 & 152.45 & 0.0 & 0.0 \\ -19.35 & 0.0 & 0.0 & 0.0 & 152.45 & 0.0 \\ 0.0 & 0.0 & 0.0 & 0.0 & 0.0 & 39.68 \end{bmatrix} \cdot 10^8 \tag{6}$$

The x- and y-directions of the system correspond to the fore-aft and side-side directions, respectively. For the earthquake shaking in the x-direction, $u_{g,x}(t)$, and earthquake shaking in the y-direction, $u_{g,y}(t)$, one would compute the kinematic interaction loads (horizontal force and moment) on the top of the pile as follows:

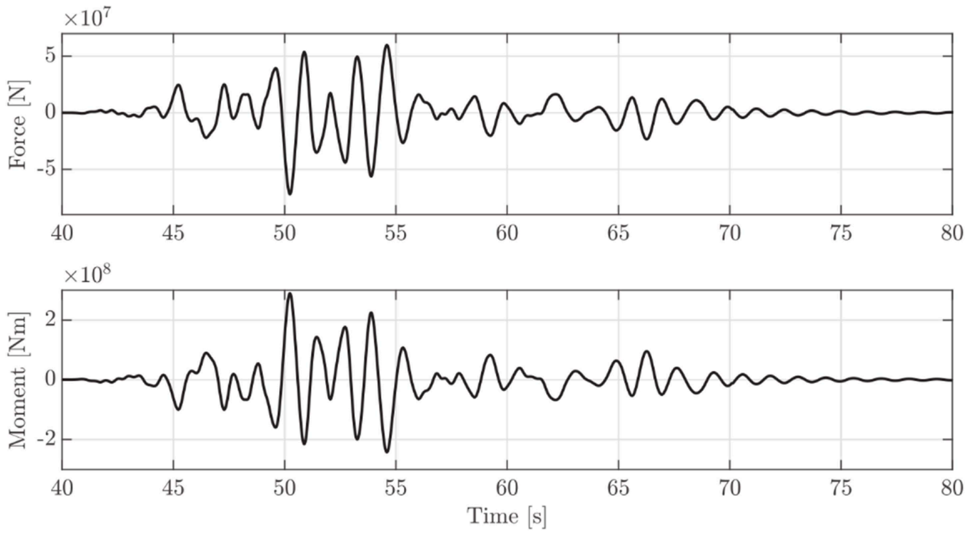

Fig. 4. Horizontal force and moment time series applied at reaction nodes for one pile. Peak horizontal force is 71,950 kN and peak moment is 289,500 kNm. Earthquake is applied at 40 s.

$$\{F_{SSI}\} = \begin{Bmatrix} F_x(t) \\ F_y(t) \\ F_z(t) \\ M_x(t) \\ M_y(t) \\ M_z(t) \end{Bmatrix} = \begin{bmatrix} K_{xx} & 0.0 & 0.0 & 0.0 & K_{x\theta_y} & 0.0 \\ 0.0 & K_{yy} & 0.0 & K_{y\theta_x} & 0.0 & 0.0 \\ 0.0 & 0.0 & K_{zz} & 0.0 & 0.0 & 0.0 \\ 0.0 & K_{\theta_x y} & 0.0 & K_{\theta_x\theta_x} & 0.0 & 0.0 \\ K_{\theta_y x} & 0.0 & 0.0 & 0.0 & K_{\theta_y\theta_y} & 0.0 \\ 0.0 & 0.0 & 0.0 & 0.0 & 0.0 & K_{\theta_z\theta_z} \end{bmatrix} \begin{Bmatrix} u_x(t) \\ u_y(t) \\ u_z(t) \\ \theta_x(t) \\ \theta_y(t) \\ \theta_z(t) \end{Bmatrix} = [K_{SSI}] \begin{Bmatrix} u_{g,x}(t) \\ u_{g,y}(t) \end{Bmatrix} \tag{7}$$

$$\begin{aligned} F_x(t) &= K_{xx} \cdot u_x(t) + K_{x\theta_y} \cdot \theta_y(t) \ ; \ M_y(t) = k_{\theta_y x} \cdot u_x(t) + k_{\theta_y\theta_y} \cdot \theta_y(t) \ ; \\ F_y(t) &= K_{yy} \cdot u_y(t) + K_{y\theta_x} \cdot \theta_x(t) \ ; \ M_x(t) = k_{\theta_x y} \cdot u_y(t) + k_{\theta_x\theta_x} \cdot \theta_x(t) \end{aligned} \tag{8}$$

The horizontal force and moment calculated by Eq. (8) for the x-direction due to the N-S acceleration time history of the Loma Prieta earthquake (Section 2.2) are shown in Fig. 4.

4. Verification

4.1. Abaqus model

The finite element model of the reference OWT was constructed in the finite element program Abaqus [37]. The model consists of five main parts; (1) tower and RNA, (2) transition piece (TP), (3) jacket, (4) piles, and (5) soil; the full assembly is referred to as the integrated model. Details of the modelling of each part, the assembling technique, damping assessment, choice of the boundary conditions, verification of the soil's dynamic response, and presentation of the model's dynamic properties are described in Pedersen and Askheim [49]. Fig. 5 shows a 3D visualization of the integrated model together with a 2D model of the soil used in the verification of the dynamic response of the soil (often referred to as *site response* in earthquake engineering terminology). The z-axis of the global coordinate system is along the tower centre axis and the x-y-plane lies at the mean sea level.

The integrated Abaqus model is used to verify the implementation of the sub-structuring method in OpenFAST. The approach is verified in the following section by comparing the earthquake response in OpenFAST against that in the Abaqus model.

4.2. Verification results

4.2.1. Natural frequencies

The mode shapes in OpenFAST are found using BModes [57] and includes the first and second fore-aft and side-side modes. The modes computed for the implemented structure is shown in Fig. 6. To highlight the effect of the substructure, plots (a) and (b) show the corresponding mode shapes if the tower is assumed clamped at the bottom (zero in the vertical axis represents the mudline).

The mode shapes calculated with BModes when the bottom of the tower is released and the mass and stiffness from the substructure are included should be like the natural frequencies of the total structure modelled in Abaqus. The natural frequencies are computed by performing two free decay analysis where the top of tower is given an initial displacement in fore-aft and side-side. During the free decay analysis, the blade's bending DOFs were turned off. This was done to ensure that the model behaves in the same manner as in Abaqus and BModes. Turning off all the bending DOFs in the blades means that the RNA will behave like a rigid body, and therefore there would be no disturbance from the blades during the free decay analysis. The gravity was also set to zero because the centre of

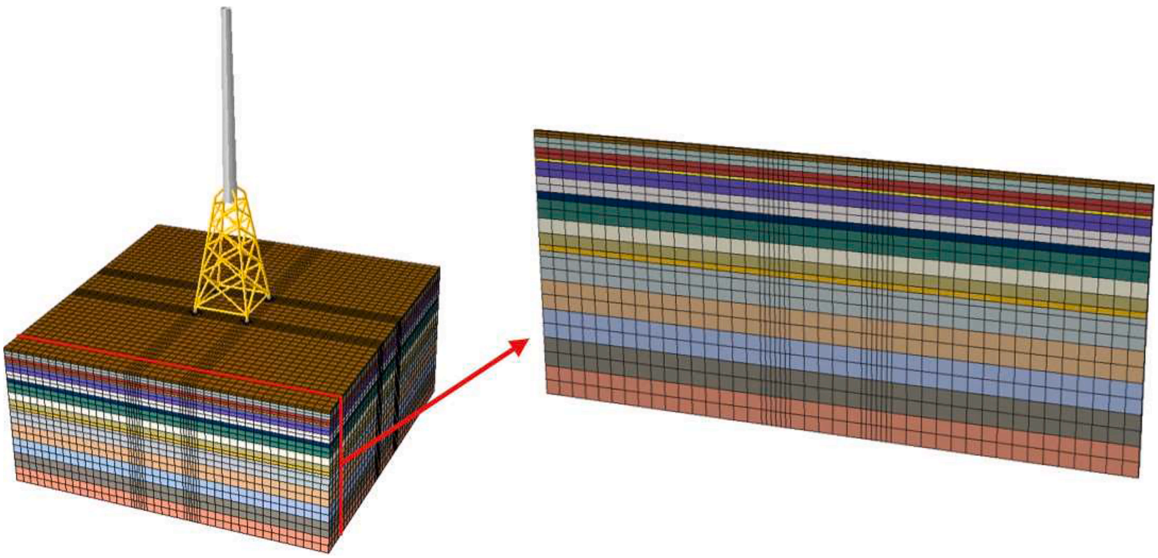

Fig. 5. Visualization of integrated model. Different colors in soil medium indicate different soil layers (Table 2).

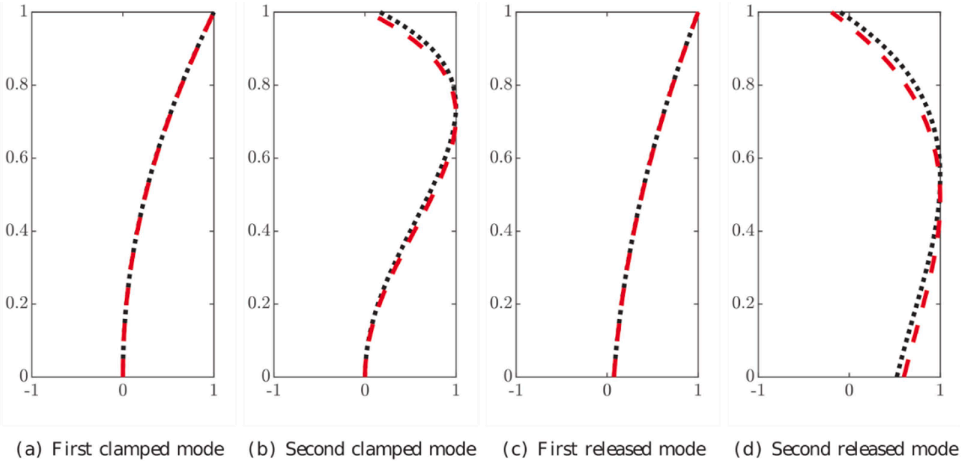

Fig. 6. Clamped and released tower mode shapes in side-side and fore-aft direction. Dashed red line indicates fore-aft and dotted black line indicates side-side.

mass of the RNA has an offset from the tower axis which would lead to a displacement and make it inconsistent to compare between the BModes and Abaqus. A Power Spectral Density (PSD) analysis of the response time series reveals the frequencies of the first modes displayed in Fig. 7. Figures (a) and (b) show that the first natural frequencies in the side-side and fore-aft directions are 0.280 Hz and 0.281 Hz, respectively. The figures also show that the second side-side and fore-aft natural frequency are respectively 1.174 Hz and 1.256 Hz. The second natural frequency is only present in the PSD of displacement for the TP and not at the top of tower. This is due to the shape of the second mode, as seen in Fig. 6(d). The tower top experiences minimal displacement during vibration in the second mode. The full support structure was simulated in Bmodes, OpenFAST and Abaqus. Table 3 summarizes the results of the three models.

The results presented in Table 3 indicate a good agreement between the BModes and OpenFAST, confirming a correct

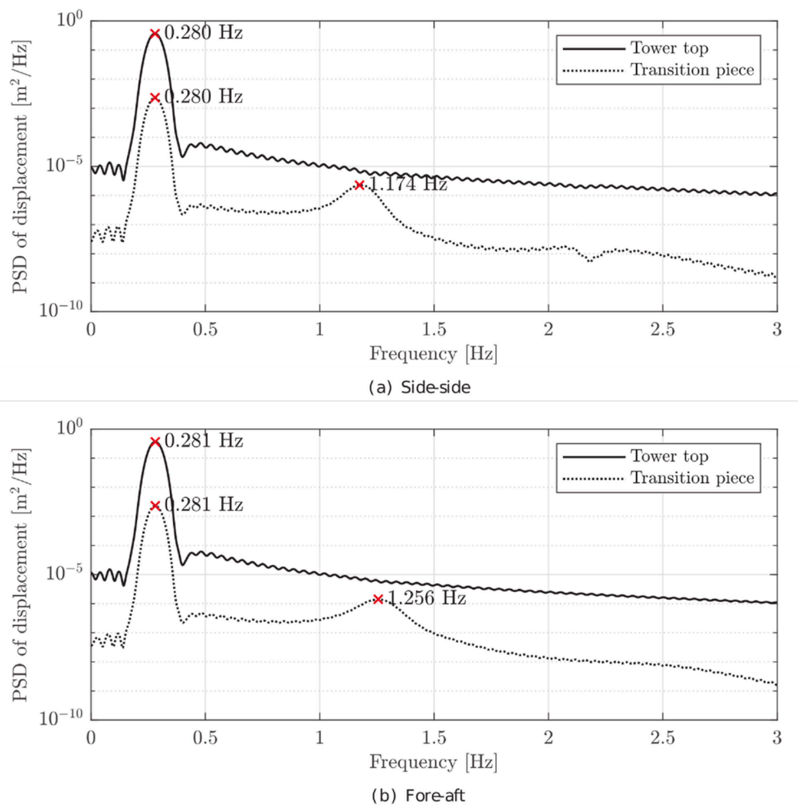

Fig. 7. PSD of displacement in side-side and fore-aft direction for TP and tower top with stiff blades.

implementation of the mode shapes. The results also show a good match with the Abaqus model, indicating a correct modelled system. The differences are believed to be due to different discretization of the system in these models.

4.2.2. Earthquake response

The earthquake response of the OpenFAST model is verified against the Abaqus model to ensure that OpenFAST handles the SSI-effects as implemented. During these calculations, earthquake is the only load applied to the models. Fig. 8 presents the comparison between the Abaqus and the OpenFAST results with both stiff and soft blade behaviour. The stiff blades are intended to represent the lumped mass assumption used in Abaqus where the RNA is assumed as a rigid body represented by a point mass and mass moment of inertia. The two blade models differ more visibly at the peaks around 10 s and 15 s. This is because the energy taken up by the soft blades damp out some of the tower's top response.

From the PSD of the response for the three models shown in Fig. 9, it can be observed that Abaqus model has a peak at the second tower fore-aft mode (1.179 Hz, see Table 3), while OpenFAST simulation does not contain this frequency at the top of tower. This is similar to the free decay analysis discussed earlier. The reason for the identification of the second natural frequency in Abaqus response is that the mode shape has a non-negligible displacement at the top of the tower, in contrast to OpenFAST mode. The mode shapes from Abaqus could have been implemented to get a greater correlation with Abaqus. The soft blade response has a peak corresponding to the second mode of the blades (1.616 Hz), which is of course not present in the stiff blade response. The response from OpenFAST model is very similar in both cases.

4.2.3. Effect of jacket on kinematic interaction

To investigate the effect of the massless jacket in the sub-structuring method, an analysis is performed in which the kinematic interaction time series are computed without the massless jacket (that is, only the piles are included in the seismic soil response). The resulting pile top forces are shown in Fig. 10, which can be compared with the results of those obtained with the massless jacket, see Fig. 4. The change in peak displacement is small compared to the change in peak rotation. The stiffness of the jacket clearly counteracts the rotation of the pile head. However, the coupling of the displacement and rotation springs gives a very small difference in the applied load. The difference between the peak load is 0.05 % in the horizontal force and 0.7 % in the moment. This indicates that the kinematic interaction forces are insensitive to presence of the jacket and the massless jacket could be disregarded in practical design. This indicates that one could derive the kinematic interaction forces by conventional simpler methods without resorting to involved numerical tools such as Abaqus.

5. Cases studies

Once the earthquake load implementation was verified, the OpenFAST model was used to simulate the following practical cases:

- **Production** - This case represents normal production during which the wind turbine is excited by both wind and waves. In this case the rotor is spinning and the OWT produces around 10MW of electricity.
- **Parked** - This case represents a parked turbine in a time with no wind. The OWT is only excited by the wave loads, as explained in Section 2.3, and the rotor is not spinning. It could be argued that the wave spectrum should be changed to a Pierson-Moskowitz spectrum since it is not a situation with developing sea state. However, because the focus of this study is on the response due to earthquake during different conditions, the same waves has been used for the ease of comparison. In this case, the DOF controlling the rotation of the rotor is fixed to prevent the rotor from rotating.
- **Maintenance** - This case represents a situation where the OWT is stopped for maintenance. In this case the OWT is excited by both wind and waves, but the rotational DOF for the rotor is the same as during the Parked case.

All the above cases have also been simulated with earthquake applied after 40 s. In the presentations, the combined loads are indicated with a plus sign, e.g., Production+EQ indicates production case with earthquake load. In addition, a separate case involving bi-directional shaking during parked condition is considered to evaluate the effect of the characteristics of the earthquake.

The focus of the analyses is the comparison of the load cases with and without earthquake load, highlighting the earthquake load effect on the structure. The considered response quantities are: 1) displacements at top of tower and TP, 2) accelerations at top of tower, and 3) overturning moment at the jacket base. The displacements are interesting both for investigation of the dynamic behaviour and the response magnitude. The tower top accelerations are interesting since it affects the workload on the RNA components, potentially leading to serviceability limitations contributing to a shorter operational lifetime of the turbine.

Fig. 11 shows the fore-aft acceleration of top of the tower when the N-S component of Loma Prieta earthquake is applied in x-

Table 3
Natural frequencies calculated with BModes and natural frequencies measured with free decay analysis.

Mode	BModes freq. [Hz]	OpenFAST freq. [Hz]	Abaqus freq. [Hz]
First side-side	0.278	0.280	0.272
First fore-aft	0.281	0.281	0.274
Second side-side	1.162	1.174	1.178
Second fore-aft	1.289	1.256	1.301

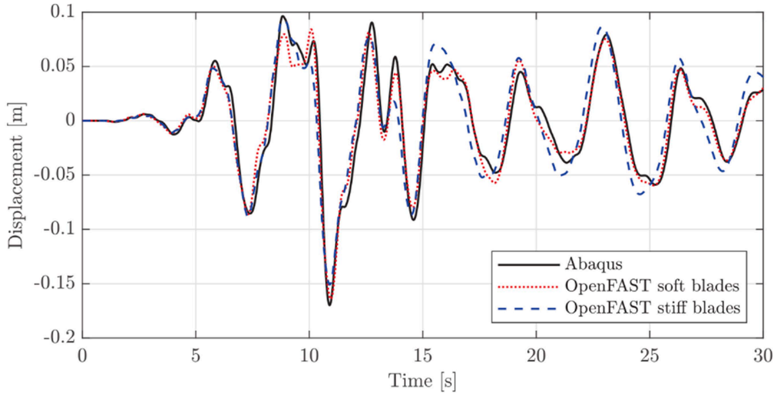

Fig. 8. Earthquake response of Abaqus fully integrated model compared to OpenFAST model with both soft and stiff blades computed at tower top.

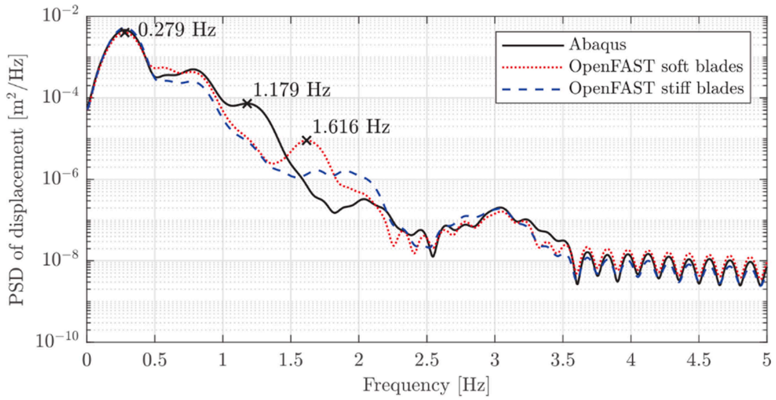

Fig. 9. Power spectral density of displacement for earthquake response of Abaqus model compared to OpenFAST with both soft and stiff blades.

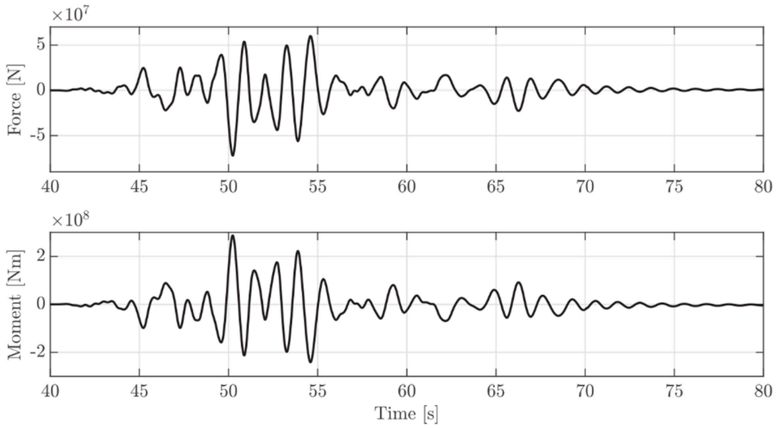

Fig. 10. Force and moment time series of kinematic interaction loads computed for only soil and piles (compare with Fig. 4). Peak force is 71,980 kN and peak moment is 287,360 kNm. Earthquake is applied at 40 s.

direction in parked conditions, and Fig. 12 shows the overturning moment for the OWT prior to and throughout the earthquake. These values serve as a reference case for the purpose of elucidating the different results obtained.

5.1. Production

Fig. 13 shows the fore-aft displacement of top of the tower and TP. The results in the top plot show that the earthquake does not

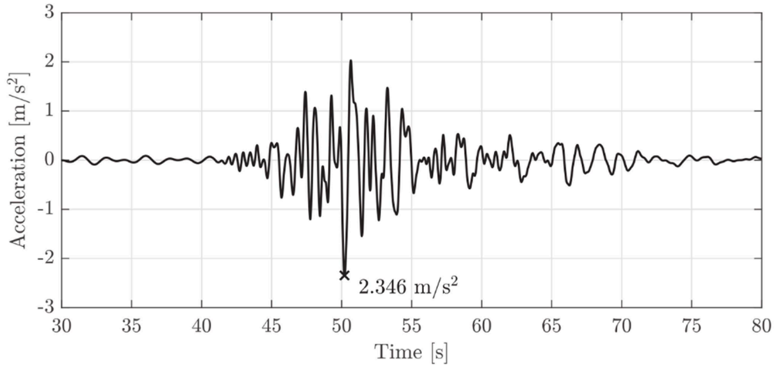

Fig. 11. Fore-aft acceleration at the top of tower during earthquake in N-S direction.

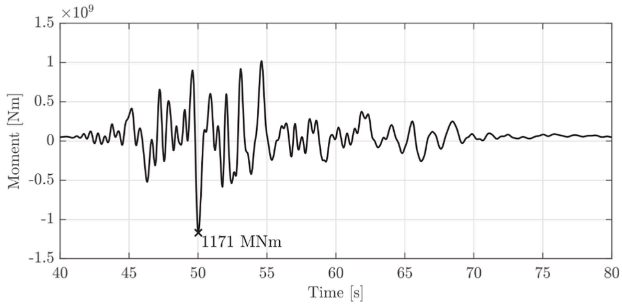

Fig. 12. Overturning moment when earthquake is applied in N-S direction.

have a big impact on the magnitude of the response at top of the tower, namely that the response only oscillates around the reference production response. This means that wind has generally a larger impact on the tower displacement compared to the earthquake. The response at the TP, however, is much larger throughout the earthquake compared to the reference production case.

Fig. 14 displays the corresponding acceleration time history on top of the tower which shows that the earthquake has a larger impact on the accelerations compared to the displacements. The results show 10 times larger accelerations during earthquake.

Fig. 15 shows the total overturning moment at the reaction nodes prior to and throughout the earthquake. It is evident that the earthquake has a large influence on the total loads acting on the structure compared to the reference production case. This should especially be investigated in a structural design setting.

5.2. *Comparing production, parked and maintenance during earthquake*

In this section, the acceleration and overturning moment in the three cases with earthquake are compared to highlight the differences. Fig. 16 shows acceleration time histories at top of tower for the most intensive 15 s of the earthquake response for the three cases which clearly demonstrates that the acceleration response is dominated by the earthquake load. Fig. 17 shows the associated overturning moments which again indicates that the earthquake has a large impact on the forces in the jacket base. The figure also shows that the difference in overturning moment amplitude between the three cases is minor, even though the Production case has an unfavourable production force applied as the force from the RNA during production has a large moment arm compared to the force from the RNA weight (overhang of the RNA). To facilitate comparison between the different operational modes employed in this study, the results obtained in the case studies are summarized in Table 4.

5.3. *Effect of earthquake characteristics*

This section investigates the response when the Loma Prieta N-S component is applied in the fore-aft direction, and the E-W component is applied in the side-side direction. The loads are applied as explained in Section 3 using Eq. (8).

Fig. 18 displays the trajectory of the tower top in the x-y-plane and shows that top of the tower experiences a displacement in the side-side (y-direction) about 2.53 times the displacement in the fore-aft (x-direction). Because the whole model has practically identical dynamic properties in the two directions, the difference is simply the result of the E-W earthquake motion being amplified by about the same factor by the E-W motion due to its frequency content being closer to the first natural frequency of the soil profile.

Fig. 19 shows that the overturning moment about the x-axis is about 3.5 times larger about the y-axis. The overturning moment about the y-direction does not noticeably change compared to the Parked+EQ case. The same magnification is also evident in the

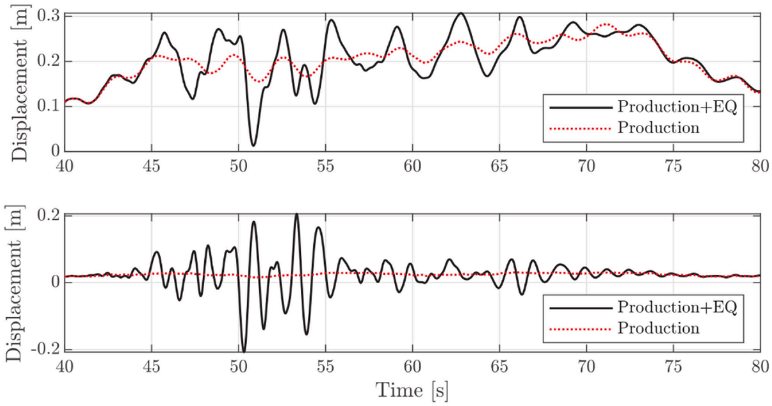

Fig. 13. Downwind displacement at top of tower (upper plot) and TP (lower plot) for production case.

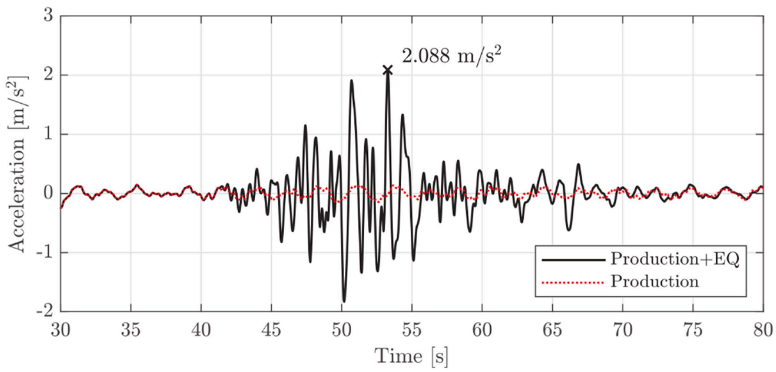

Fig. 14. Fore-aft acceleration at top of tower during earthquake for production case.

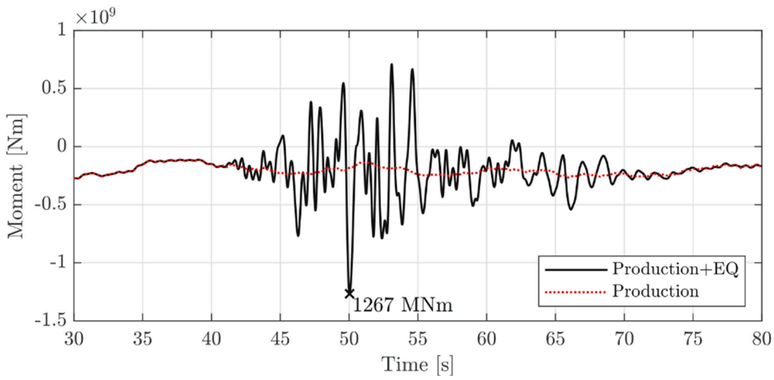

Fig. 15. Overturning moment for production case during earthquake.

accelerations in the side-side direction as shown in Fig. 20.

It should be noted that while only one acceleration time history has been used in this study to assess the relative order of earthquake shaking, in practical design it is common to use a suite of representative time histories to capture the variability/uncertainty in the characteristics of the time histories in the seismic design assessment.

6. Consideration of soil non-linearity

In earthquake SSI analyses it is common to speak of two types of nonlinearities related to soil response: a) primary nonlinearity, which is due to the soil nonlinearity due the seismic wave propagation though the soil layer (i.e. in the absence of foundation and

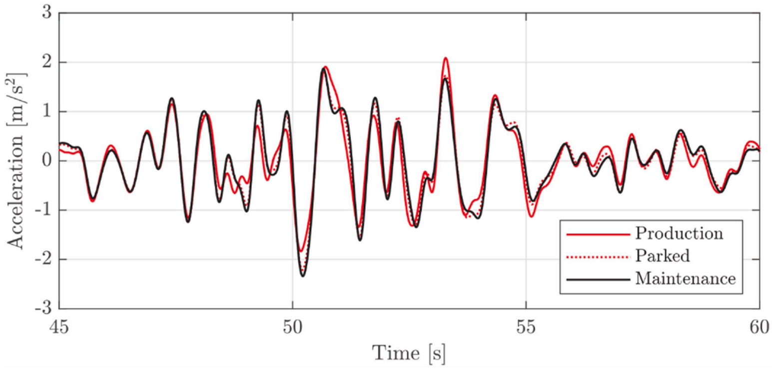

Fig. 16. Acceleration at top of tower for the three cases during earthquake on an enlarged time scale.

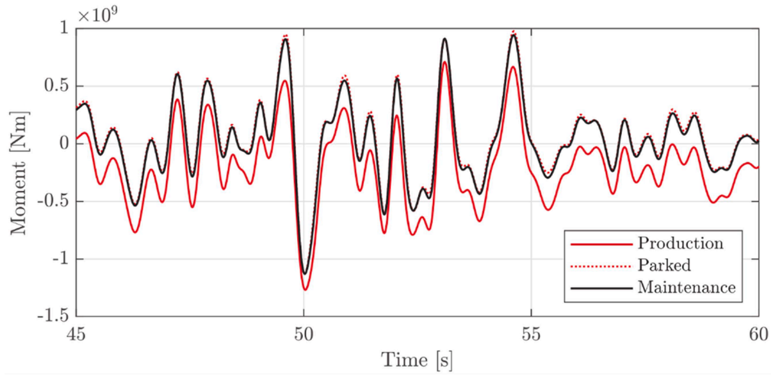

Fig. 17. Overturning moment for the three considered cases during earthquake on an enlarged time scale.

Table 4
Summary results for comparison between cases.

Cases studies	Production	Parked	Maintenance
Displacement at top of tower [m]	0.310	0.380	0.366
Displacement at transition piece [m]	0.207	0.247	0.242
Acceleration at top of tower [m/s^2]	2.088	2.341	2.345
Overturning moment [MN/m]	1267	1130	1129

structure), and b) secondary nonlinearity which arises due the dynamic loads from the oscillating structure (often referred to as inertial interaction loads). The described sub-structuring procedure in the above sections can be used to capture the primary nonlinearity. This can be achieved by using the acceleration time histories on the seabed from a conventional nonlinear site response analysis and computing the foundation impedances/springs by using the strain-compatible shear moduli of the soil derived from the site response analysis. While this approach often conservatively reflects the seismic response and forces in the structure, it is unable to capture secondary nonlinear response feature if they are not minor. Examples are soils that can liquefy during earthquake shaking and soft soils that yield under the combined stresses from the earthquake and structural response. While specialized numerical tools are required for the first example (liquefaction) [58,59], it is rather straightforward to evaluate if the secondary nonlinearity is an issue for the second example. In this case, an assessment can be made by comparing the stresses at the soil-foundation interface with the soil yield stress. In the case of jackets on piles, the secondary nonlinearity can lead to unequal penetration of the piles in the soil and the ensuing permanent tilt of the jacket if the OWT is simultaneously exposed to the environmental loads, especially the wind load as it tends to exert the largest axial loads in the piles. For such cases, one must resort to fully nonlinear models with proper constitutive soil models, for example using Abaqus.

The Abaqus model used in this study was used to highlight the above point. To this end, the constructed integrated Abaqus model with non-linear soil behaviour according to the Mohr-Coulomb plasticity model was employed under three load cases:

- **Load Case I** – Earthquake excitation in x-direction by the Loma Prieta N-S time history, and a 2MN concentrated force in x-direction at top of tower approximately representing wind load.

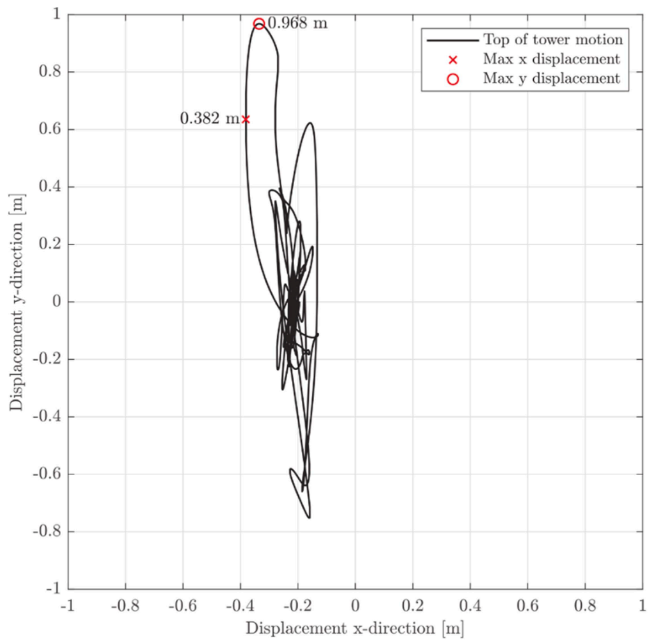

Fig. 18. Motion of tower top during earthquake applied in both directions.

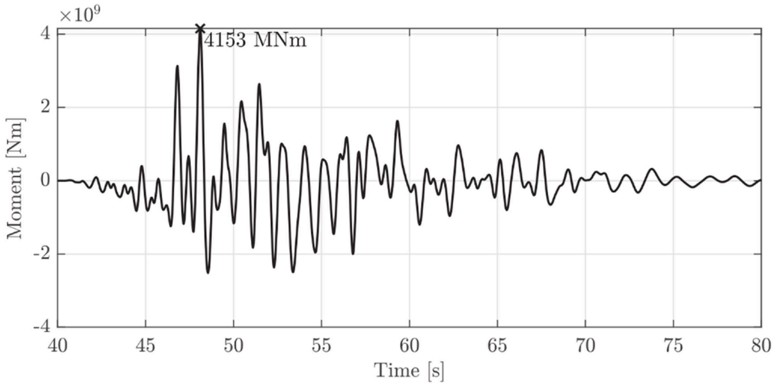

Fig. 19. Overturning moment about x-axis when earthquake is applied in both directions.

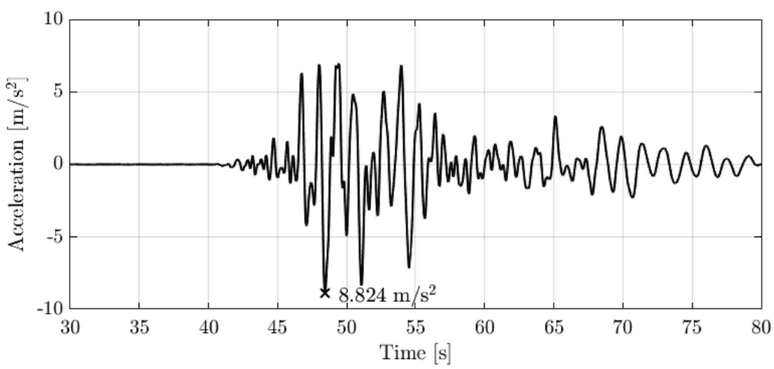

Fig. 20. Side-side acceleration at the top of tower during earthquake in both directions.

- **Load Case II** – Earthquake excitation in x-direction by the Loma Prieta N-S accelerations magnified by a factor of 3, and the same concentrated force as in LC I.
- **Load Case III** – Earthquake excitation in x-direction by the Loma Prieta N-S time history together with earthquake excitation in y-direction by the Loma Prieta E-W time history together with the same concentrated force as in LC I.

The concentrated force is simulating an average production force from the RNA. The force is considered constant over time, as the wind-induced production forces is roughly static during the short earthquake excitation. No other environmental loads are applied. The choice of load cases aims to show how earthquake shaking together with wind affect the tilt and its accumulation during earthquake loading.

Fig. 21 shows the computed tilt of the jacket for the three load cases. The analysis was performed in three steps: 1) applying the static gravity loading, 2) applying the static wind load and performing the earthquake analysis including non-linear soil behaviour and 3) performing a free vibration (decay) analysis to reach a permanent state.

As expected, LC II with a three-fold acceleration increase has resulted in the largest tilt. Even the tilt from LC I exceeds the allowable tilt of 0.05 degrees [24] for this earthquake which should be noted that it is a relatively strong earthquake event.

To illustrate the accumulation of tilt, the vertical shear stress, τ_{xz}, during load case II is plotted for selected elements along the pile-soil interface in Fig. 22. Every moment during the shaking the shear stress exceeds the soil's shear strength, the pile slips relative to the soil. Time histories of the shear stresses with stress yield plateaus, especially those with low shear strength closer to the seabed, clearly demonstrate the mechanism of gradual tilt development in jacket structures. The objective of these analyses has been to present and point out the need for advanced FE tools for modelling of highly nonlinear soil response which might lead to permanent tilting and/or sinking of a tower structure. Therefore, no attempt has been made to improve the accuracy of the results by, for example, refining the FE mesh or using other constitutive soil models.

7. Summary and conclusions

In this paper, the implementation of SSI-effects in the computational software OpenFAST with the use of a multi-step method and a complementary integrated Abaqus model is shown and verified. OpenFAST is a custom made, advanced and efficient software for hydro-aero-servo-elasto-dynamic analyses of wind turbines. The turbine and jacket structure studied is an offshore wind turbine based on the IEA 10 MW reference OWT founded on the piles designed for the reference jacket designed in the European research project INNWIND. To compute the earthquake excitation forces as input to the OpenFAST model, kinematic interaction displacements are extracted from the Abaqus model including the piles and massless structure. The inclusion of the massless jacket is investigated, and the results show negligible effect. Thus, if the jacket geometry is not available in the geotechnical model, the jacket could be neglected for the kinematic force computations. Comparing the earthquake responses, the OpenFAST model reproduces the results from the Abaqus integrated model satisfactorily. Therefore, it is shown that OpenFAST model with the implemented kinematic interaction forces and foundation springs is able to accurately simulate the earthquake loading. The present methodology is primarily developed to facilitate the accessibility of seismic analysis to OpenFAST users. The developed methodology allows the introduction of seismic loads directly in OpenFAST through the ServoDyn module and enables consideration of seismic loads simultaneously with other environmental loads.

With the OpenFAST model, different cases including combined effect of environmental and earthquake loading is simulated. The analyses reveal that the operational wind-induced forces dominate the displacements at top of the tower, while the earthquake

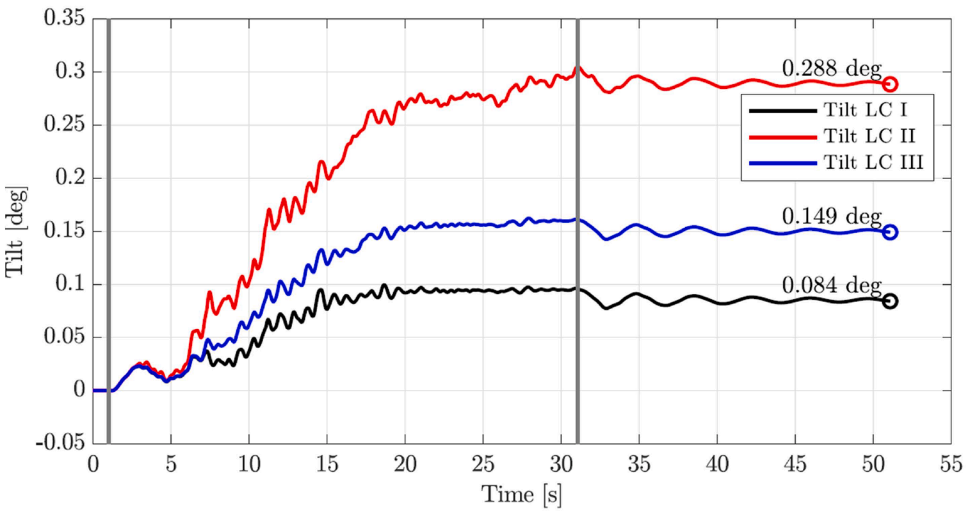

Fig. 21. Tilt for all load cases (LC). Permanent tilt after decay highlighted with number. Grey vertical lines indicating step separation.

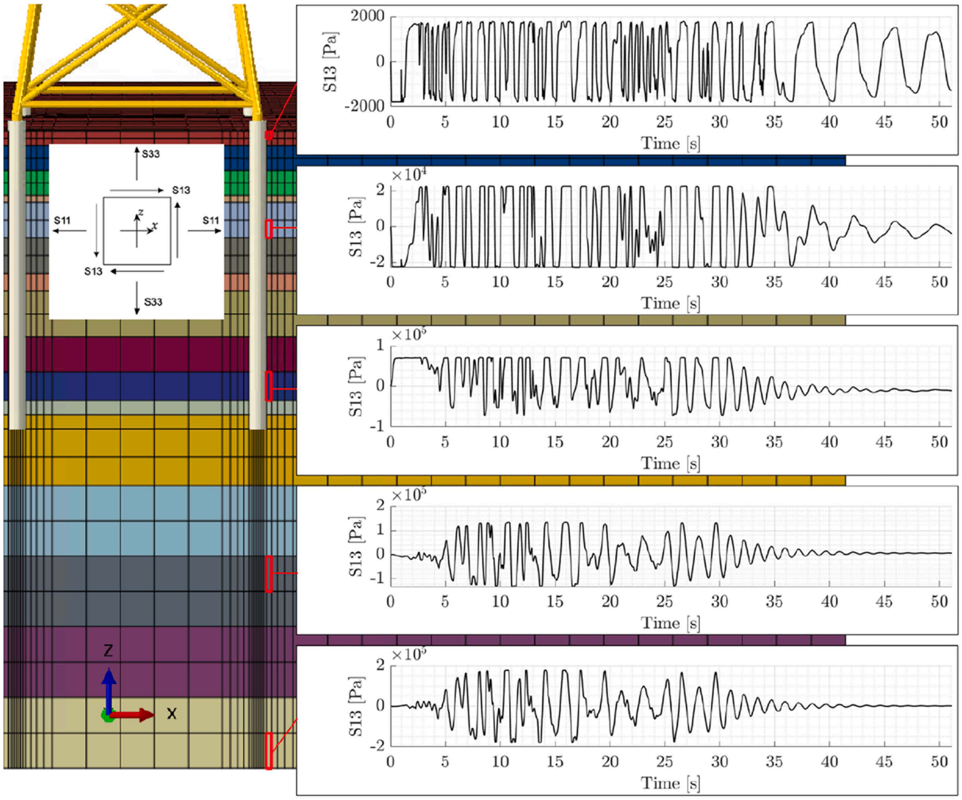

Fig. 22. Vertical shear stresses for chosen elements during Load Case II. S11 = σ_x, S33 = σ_z and S13 = τ_{xz} . (Note: Abaqus positive stress convention for the x-z plane shown to the left).

dominates accelerations at top of the tower and the overturning moment at the jacket base. This indicates necessity of including earthquake loading in at least moderate seismic environments. A limited set of analyses using the nonlinear soil model in Abaqus are performed which illustrate the importance of performing nonlinear dynamic analyses if there is indication of non-negligible secondary soil nonlinearity which could result in permanent tilt in jacketed OWTs. It should be noted that when earthquake shaking is expected to have an impact on the loads, a suite of representative time histories should be used in typical design to capture the variabilities in the earthquake characteristics.

CRediT authorship contribution statement

Amir M. Kaynia: Writing – review & editing, Validation, Supervision, Methodology, Conceptualization. **Daniel Martens Pedersen:** Writing – original draft, Validation, Software, Methodology, Formal analysis. **Henrik Askheim:** Writing – original draft, Validation, Software, Methodology, Formal analysis. **Carlos Romero-Sánchez:** Writing – review & editing.

Declaration of competing interest

The authors declare that they have no known competing financial interests or personal relationships that could have appeared to influence the work reported in this paper.

Acknowledgments

This paper is based partly on the MSc thesis of the second and third authors at the Department of Structural Engineering, Norwegian University of Science and Technology (NTNU) [49]. The fourth author acknowledges the research fellowship (TESIS2022010011) given by ACIISI of the *Consejería de Economía, Conocimiento y Empleo of the Gobierno de Canarias* and *FSE*, which made it possible for him to contribute to this paper during a short–term research visit at NGI in 2024. The authors would like to thank Jason Jonkman and Andy Platt at NREL for they valuable comments during the implementation of the developed method in OpenFAST.

Data availability

No data was used for the research described in the article.

References

[1] Yang Y, Bashir M, Li C, Wang J. Analysis of seismic behaviour of an offshore wind turbine with a flexible foundation. Ocean Eng 2019;178:215–28.
[2] Shi S, Zhai E, Xu C, Iqbal K, Sun Y, Wang S. Influence of pile-soil interaction on dynamic properties and response of offshore wind turbine with monopile foundation in sand site. Appl Ocean Res 2022;126:103279.
[3] Álamo GM, Aznárez JJ, Padrón LA, Martínez-Castro AE, Gallego R, Maeso O. Dynamic soil-structure interaction in offshore wind turbines on monopiles in layered seabed based on real data. Ocean Eng 2018;156:14–24.
[4] Kaynia AM. Effect of kinematic interaction on seismic response of offshore wind turbines on monopiles. Earthq Eng Struct Dyn 2021;50(3):777–90.
[5] Medina C, Álamo GM, Padrón LA. Contribution of the rotational kinematic interaction to the seismic response of monopile-supported offshore wind turbines. Ocean Eng 2023;280:114778.
[6] Kaynia AM, Kausel E. Dynamics of piles and pile groups in layered soil media. Soil Dyn Earthq Eng 1991;10(8):386–401.
[7] Gazetas G, Fan K, Kaynia A, Kausel E. Dynamic interaction factors for floating pile groups. J Geotech Eng 1991;117(10):1531–48.
[8] Padrón L, Aznárez J, Maeso O. BEM-FEM coupling model for the dynamic analysis of piles and pile groups. Eng Anal Bound Elem 2007;31(6):473–84.
[9] Damgaard M, Zania V, Andersen LV, Ibsen LB. Effects of soil–structure interaction on real time dynamic response of offshore wind turbines on monopiles. Eng Struct 2014;75:388–401.
[10] Carbonari S, Morici M, Dezi F, Leoni G. A lumped parameter model for time-domain inertial soil-structure interaction analysis of structures on pile foundations. Earthq Eng Struct Dyn 2018;47(11):2147–71.
[11] Andersen LV. Dynamic soil–structure interaction of polypod foundations. Comput Struct 2020;232:105966.
[12] Zaaijer M. Foundation modelling to assess dynamic behaviour of offshore wind turbines. Appl Ocean Res 2006;28(1):45–57.
[13] Arany L, Bhattacharya S, Macdonald JH, Hogan SJ. Closed form solution of Eigen frequency of monopile supported offshore wind turbines in deeper waters incorporating stiffness of substructure and SSI. Soil Dyn Earthq Eng 2016;83:18–32.
[14] Jalbi S, Bhattacharya S. Closed form solution for the first natural frequency of offshore wind turbine jackets supported on multiple foundations incorporating soil-structure interaction. Soil Dyn Earthq Eng 2018;113:593–613.
[15] Liang F, Yuan Z, Liang X, Zhang H. Seismic response of monopile-supported offshore wind turbines under combined wind, wave and hydrodynamic loads at scoured sites. Comput Geotech 2022;144:104640.
[16] Bisoi S, Haldar S. Design of monopile supported offshore wind turbine in clay considering dynamic soil–structure-interaction. Soil Dyn Earthq Eng 2015;73:103–17.
[17] API. Recommended practice 2A-WSD planning, designing, and constructing fixed offshore platforms - working Stress design. American Petroleum Institute; 2014.
[18] Krathe V, Kaynia AM. Implementation of a non-linear foundation model for soil-structure interaction analysis of offshore wind turbines in FAST. Wind Energy 2017;20(4):695–712.
[19] Jonkman J.M., Buhl M.L., others. *FAST user's guide*. 365. National Renewable Energy Laboratory Golden, CO, USA, 2005.
[20] Iwan WD. On a class of models for the yielding behavior of continuous and composite systems. J Appl Mech 1967;34(3):612–7.
[21] Bergua R, Robertson A, Jonkman J, et al. OC6 Phase II: integration and verification of a new soil–structure interaction model for offshore wind design. Wind Energy 2022;25(5):793–810.
[22] OpenFAST documentation. National Renewable Energy Laboratory; 2024. *Release v3.5.2*, https://openfast.readthedocs.io/en/main/. Code published at h t t p s : / / github. com/OpenFAST/openfast.
[23] Page AM, Grimstad G, Eiksund GR, Jostad HP. A macro-element pile foundation model for integrated analyses of monopile-based offshore wind turbines. Ocean Eng 2018;167:23–35.
[24] Kaynia AM. Seismic considerations in design of offshore wind turbines. Soil Dyn Earthq Eng 2019;124:399–407.
[25] Kjørlaug RA, Kaynia AM. Vertical earthquake response of megawatt-sized wind turbine with soil-structure interaction effects. Earthq Eng Struct Dyn 2015;44(13):2341–58.
[26] Asareh MA, Schonberg W, Volz J. Effects of seismic and aerodynamic load interaction on structural dynamic response of multi-megawatt utility scale horizontal axis wind turbines. Renew Energy 2016;86:49–58.
[27] Mo R, Kang H, Li M, Zhao X. Seismic fragility analysis of monopile offshore wind turbines under different operational conditions. Energies 2017;10(7):1037.
[28] Padrón LA, Carbonari S, Dezi F, Morici M, Bordón JD, Leoni G. Seismic response of large offshore wind turbines on monopile foundations including dynamic soil–structure interaction. Ocean Eng 2022;257:111653.
[29] Gelagoti FM, Kourkoulis RS, Georgiou IA, Karamanos SA. Soil-structure interaction effects in offshore wind support structures under seismic loading. J Offshore Mech Arctic Eng 2019;141(6):061903.
[30] Ngo DV, Kim DH. Seismic responses of different types of offshore wind turbine support structures. Ocean Eng 2024;297:117108.
[31] Alati N, Failla G, Arena F. Seismic analysis of offshore wind turbines on bottom-fixed support structures. Philos Trans R Soc A Math Phys Eng Sci 2015;373(2035):20140086.
[32] Bossanyi E. Bladed for windows user manual. Bristol, UK: Garrad Hassan and Partners; 2000. p. 405.
[33] Abhinav K, Saha N. Coupled hydrodynamic and geotechnical analysis of jacket offshore wind turbine. Soil Dyn Earthq Eng 2015;73:66–79.
[34] Ku CY, Chien LK. Modeling of load bearing characteristics of jacket foundation piles for offshore wind turbines in Taiwan. Energies 2016;9(8):625.
[35] Ju SH, Huang YC. Analyses of offshore wind turbine structures with soil-structure interaction under earthquakes. Ocean Eng 2019;187:106190.
[36] James M, Haldar S. Seismic vulnerability of jacket supported large offshore wind turbine considering multidirectional ground motions. Structures 2022;43:407–23.
[37] Dassault Systèmes. Abaqus. Available online: https://bit.ly/3qzjGwk; 2021.
[38] Romero-Sánchez C, Padrón L. Influence of wind and seismic ground motion directionality on the dynamic response of four-legged jacket-supported Offshore Wind Turbines. Eng Struct 2024;300:117191.
[39] Plodpradit P, Dinh VN, Kim KD. Coupled analysis of offshore wind turbine jacket structures with pile-soil-structure interaction using FAST v8 and X-SEA. Appl Sci 2019;9(8):1633.
[40] Yan Y, Yang Y, Bashir M, Li C, Wang J. Dynamic analysis of 10 MW offshore wind turbines with different support structures subjected to earthquake loadings. Renew Energy 2022;193:758–77.
[41] Hussan M, Rahman MS, Sharmin F, Kim D, Do J. Multiple tuned mass damper for multi-mode vibration reduction of offshore wind turbine under seismic excitation. Ocean Eng 2018;160:449–60.
[42] Romero-Sánchez C, Padrón L. Seismic response of jacket-supported offshore wind turbines for different operational modes considering earthquake directionality. Ocean Eng 2024;311:118798.
[43] Damiani R, Jonkman J, Hayman G. SubDyn user's guide and theory manual. Golden, CO (United States): National Renewable Energy Laboratory(NREL); 2015. tech. rep.
[44] Wang L, Ishihara T. A new FounDyn module in OpenFAST to consider foundation dynamics of monopile supported wind turbines using a site-specific soil reaction framework. Ocean Eng 2022;266:112692.

[45] Bortolotti P, Dykes K, Merz K, Zahle F. IEA wind task 37 on systems engineering in Wind energy – WP2.1 reference Wind turbines. International Energy Agency; 2019. Available online: https://www.nrel.gov/docs/fy19osti/73492.pdf.

[46] Bak C, Zahle F, Bitsche R, et al. Description of the DTU 10 MW reference wind turbine. In: DTU Wind Energy Report-I-0092. 5; 2013.

[47] Borstel (Ramboll) vT. Design report – reference jacket INNWIND.EU. Deliverable 4.3.1. Available online: http://www.innwind.eu/publications/deliverable-reports; 2013.

[48] Ramboll. Interface document for prelimenary jacket design. INNWIND.EU - –10MW jacket. Available online: http://www.innwind.eu/publications/deliverable-reports; 2013.

[49] Pedersen DM, Askheim H. Implementation of seismic soil-structure interaction in OpenFAST and application to a 10MW offshore wind turbine on jacket structure. MS Thesis. Norwegian University of Science and Technology; 2021.

[50] NGA-West2 ground motion database. Pacific Earthquake Engineering Research Center (PEER); 2022. Available online: ngawest2.berkeley.edu/. Accessed on 20 April 2021.

[51] Jonkman J, Hayman B, Jonkman B, Damiani R, Murray R. AeroDyn v15 user's guide and theory manual. Golden, CO (United States): National Renewable Energy Laboratory (NREL); 2015. tech. rep.

[52] Jonkman B. TurbSim user's guide v2. 00.00 draft version. Golden, CO, USA: National Renewable Energy Laboratory; 2016.

[53] Jonkman JM, Robertson A, Hayman GJ. HydroDyn user's guide and theory manual. National Renewable Energy Laboratory; 2014.

[54] Chopra AK. Dynamics of structures: theory and application to earthquake engineering. Prentice-Hall international series in civil engineering and engineering mechanics. 4th ed. Pearson Education; 2012.

[55] Craig Jr RR, Bampton MC. Coupling of substructures for dynamic analyses. AIAA J 1968;6(7):1313–9.

[56] Jonkman J. Overview of the servodyn control & electrical-drive module. National Renewable Energy Laboratory (NREL); 2014. p. 11–2.

[57] Bir G. User's guide to BModes (software for computing rotating beam-coupled modes). Golden, CO (United States): National Renewable Energy Laboratory (NREL); 2005. tech. rep.

[58] Madabhushi GSP. Pile foundations in liquefiable soils. In: Kaynia AM, editor. Chapter 9 in analysis of pile foundations subject to static and dynamic load. London: CRC Press; 2021.

[59] Esfeh PK, Kaynia AM. Earthquake response of monopiles and caissons for Offshore Wind Turbines founded in liquefiable soil. Soil Dyn Earthq Eng 2020;136 (2020):106213. https://doi.org/10.1016/j.soildyn.2020.106213.